Journal of Molecular Catalysis A: Chemical 424 (2016) 45–53

Contents lists available at ScienceDirect

Journal of Molecular Catalysis A: Chemical

journal homepage: www.elsevier.com/locate/molcata

Visible light photocatalytic reduction of Cr(VI) by surface modified CNT/titanium dioxide composites nanofibers

Alaa Mohamed[a,c,*], T.A. Osman[b], M.S. Toprak[a], M. Muhammed[a], Eda Yilmaz[d], A. Uheida[a,*]

[a] Department of Materials and NanoPhysics, KTH –Royal Institute of Technology, SE 16440, Stockholm, Sweden
[b] Mechanical Design and Production Engineering Department, Cairo University, 12613 Giza, Egypt
[c] Production Engineering and Printing Technology Department, Akhbar El Yom Academy, 12655 Giza, Egypt
[d] National Nanotechnology Research Center, Bilkent University, 06800 Ankara, Turkey

ARTICLE INFO

Article history:
Received 26 June 2016
Received in revised form 22 July 2016
Accepted 11 August 2016
Available online 12 August 2016

Keywords:
Photocatalytic reduction
Chromium (VI)
Composite nanofibers
Visible light

ABSTRACT

In this work we report a highly efficient photocatalytic reduction of Cr(VI) based on PAN-CNT/TiO_2-NH_2 composite nanofibers fabricated by using electrospinning technique followed by chemical crosslinking of surface modified TiO_2 NPs functionalized with amino group. The structure and morphology of the fabricated composite nanofibers were characterized by FTIR, SEM, TEM, TGA, and XPS. The results indicate that the composite nanofibers possess excellent photoreduction performance for Cr(VI) under visible light (125 W) after 30 min, which is much faster than previous reports. The effects of various experimental parameters such as catalyst dose, irradiation time, initial concentration of Cr(VI), and pH on the photoreduction efficiency of Cr(VI) were investigated. The highest photoreduction efficiency of Cr (VI) was obtained at low acidity and low amount of TiO_2/CNT photocatalyst. The kinetic experimental data was attained and fitted well with a pseudo-first-order model. The UV–vis spectrophotometer and XPS analyses proved that chromate Cr(VI) was reduced to Cr(III). In addition, it can be concluded that the addition of the phenol enhances the photocatalytic reduction of Cr(VI). Furthermore, the photoreduction mechanism has also been discussed. Finally, the fabricated composite nanofibers were found to be stable after at least five regeneration cycles.

1. Introduction

Chromium plays an essential role in plant and animal metabolism, and is widely used in many industrial processes such as electroplating, textile dyeing, paint, leather tanneries, and pigment industries as critical industry materials [1]. Cr exists mainly in hexavalent Cr(VI) and trivalent Cr(III) forms in the natural environment [2]. The hexavalent chromium Cr(VI) is highly toxic and carcinogenic to humans, animals, and plants. The World Health Organization (WHO) recommends the maximum allowable limit for the discharge of Cr(VI) into inland surface water is 0.1 ppm, and into the drinking water is 0.05 ppm. Therefore, the preferred treatment is a reduction of Cr(VI) to the less harmful Cr(III), in order to avoid the deleterious impact of the Cr(VI) on the human health. Toxicity of Cr(III) is relatively low and it is one of the essential micronutrient for human health [3]. In reality, industrial wastewater consists of a mixture of organic and inorganic pollutants. Therefore, phenolic compounds are used as a model pollutant because they are widely used in the preparation of resins, herbicides, and fungicides which are highly toxic to most aquatic life [4,5]. Therefore, there is an urgent need to remove phenol from the wastewater.

Hence, the reduction of Cr(VI) into Cr(III) received great attention in the environmental remediation processes. Different techniques have been reported for the treatment of Cr(VI) pollution including chemical reduction, ion exchange, sorption, photocatalytic, and bacterial reduction [6–10]. However, most of these methods require either high energy or large quantities of chemicals and are not widely used [8,9]. Recently, the photocatalytic processes have received considerable attention because being economically viable, facile, and effective method for a rapid efficient destruction of environmental pollutants [11,12]. Many semiconductor catalysts, such as TiO_2, ZnO, ZnS, ZrO_2, CdS and WO_3, have been studied to investigate the photocatalytic reduction of Cr(VI) to Cr(III) [13–19]. Among various semiconductor catalysts, TiO_2 was considered as one of the most promising candidates due to its opti-

* Corresponding author.
E-mail addresses: alakha@kth.se (A. Mohamed), salam@kth.se (A. Uheida).

http://dx.doi.org/10.1016/j.molcata.2016.08.010
1381-1169/

cal and electronic properties, low cost, high level of photocatalytic activity, chemical stability and non-toxicity [20], which provides attractive applications to the photocatalytic reaction. Moreover, an addition of CNT to the photocatalytic materials shows higher electron conducting ability and higher adsorption capacity, which means they can act as promising materials for environmental clean-up applications [21]. CNT and TiO_2 act as an electron donor, thus stabilizing the charge carriers and preventing the charge recombination and also enabling the activity of TiO_2 photocatalytic in the visible light region and have been proven to have an excellent photocatalytic performance in photodecomposition [22].

The separation of the photocatalytic powder from the treated solution after reaction is essential, because it is difficult to separate and recover after processing with wastewater, causing secondary pollution and this process is time consuming and costly, which limits its application for water purification. Therefore, researchers are focusing on the development of polymer based composite materials, mainly by incorporation or deposition of metal or semiconductor and metal semiconductor NPs in/on polymeric nanofibers due to their enhanced properties and potential application in catalysis and environmental remediation [23–25]. In this regard, electrospinning technique is an economic and effective way of synthesizing polymer nanofibers [26,27], which display large specific surface area, fine fabric structure, high aspect ratio, flexible surface functionality, tunable surface morphologies and better adsorption as well as filtration properties [28,29]. Polyacrylonitrile (PAN) is the most widely used polymer for manufacturing high performance fibers due to its excellent characteristics and commercial availability, as well as its non-toxic nature [30]. According to our knowledge, few studies working on the reduction of Cr(VI) under visible light irradiation using nanocomposites materials [31–35]. These studies have a lot of problem like longer irradiation time (2–4 h) and high power intensity (>125 W) to obtain the maximum reduction.

In this work, we develop a new system based on composite nanofibers consisting of PAN, and CNT fabricated using an electrospinning technique followed by further crosslinking of surface amino-modified TiO_2 NPs to these PAN/CNT nanofibrous matrices in order to increase the adsorption of heavy metals due to the large number of binding active sites incorporated on the surface of TiO_2 NPs. Our previous work verifies the success of this system under UV and visible light irradiation compared to earlier reports [36,37]. The objectives of this study were to fabricate composite nanofibers containing PAN polymer, MWCNT, and surface amino-modified TiO_2 NPs and to develop an efficient and economic photocatalytic composite nanofibers for the photoreduction of Cr(VI) in aqueous solutions under visible light irradiation. The effect of operating parameters includes initial solution pH, the amount of photocatalyst, and Cr(VI) concentration on the photocatalytic reduction of Cr(VI) were investigated. Furthermore, the synergistic photocatalytic mechanism has also been discussed.

2. Experimental

2.1. Materials

Polyacrylonitrile, PAN (MW = 150,000); *N,N*-dimethylformamide (DMF), sodium hydroxide (NaOH) and hydrochloric acid (HCl), titanium dioxide powder (TiO_2 Degussa P-25), and 3-aminopropyltriethoxysilane (APTES), were purchased from Sigma Aldrich. Multi-walled carbon nanotubes, MWCNTs (purity 95 wt%; diameter: 10–40 nm; length: 20 μm; specific surface area 460 m^2/g) were synthesized and the procedure is described elsewhere [38]. Potassium dichromate ($K_2Cr_2O_7$), and caffeic acid (3,4-dihydroxycinnamic acid, 99%) were purchased from Sigma Aldrich. All reagents and solvents were of analytical reagent grade and used as received from commercial suppliers.

2.2. Catalyst preparation and characterization

Polyacrylonitrile (PAN) was dissolved in *N,N*-dimethylformamide (DMF) (10 wt.%), at 50 °C for 4 h. Then a desired amount of functionalized CNTs was added into PAN solution. Finally, the solution was stirring for 15 min and then sonicated for 2 h to completely dissolved. The above solution was loaded into a syringe pump with a flow rate 0.5 mL/h, at 25 kV. The fibers were collected on the alumina foil and then dried to remove the excess solvent. In addition, the surface functionalization of TiO_2 nanoparticles with the amino group was carried out according to a well-established procedure described in Ref. [39]. The crosslinking of the PAN/CNT composite nanofibers to TiO_2-NH_2 NPs was carried out as described elsewhere [36].

The morphology of the composite nanofibers was examined using Scanning Electron Microscopy (SEM, Gemini Zeiss-Ultra 55) and Transmission Electron Microscopy (TEM, JEM-2100F, Joel). Fourier transform infrared spectroscopy (FTIR, Nicolet iS10) was used to indicate the spectra of PAN and PAN-CNT/TiO_2-NH_2 composite nanofibers before and after Cr(VI) reduction. The thermal stabilities of the composite nanofiber samples were determined by using thermogravimetric analysis (TGA), TGA Q500, TA instrument. This was done by heating the sample from room temperature until 800 °C with a heating rate of 20 °C min^{-1} under synthetic air. The concentration of Cr (VI) in the solution was measured using UV–vis/NIR spectrophotometer (model LAMBDA 750, Perkin Elmer). Surface chemical compositions of PAN-CNT/TiO_2-NH_2 composite nanofibers were analyzed using Thermo Scientific K-Alpha x-ray photoelectron spectrometer with monochromated Al Kα radiation. Sample surface was neutralized against charging with flood gun emission during the measurements and all the spectra were corrected according to the C 1 s peak against additional charging effects.

2.3. Photocatalytic reduction experiments

Photocatalytic experiments were conducted in a column (2 cm diameter, 30 cm height) in which composite nanofibers mat of 5 cm × 5 cm was placed in the middle of the column. A 30 mL aliquot of Cr(VI) with initial Cr(VI) concentration of 20 mg/L was used. The column was shaking at room temperature for 30 min and covered from any source of light to assure that the adsorption equilibrium of Cr(VI) was reached. The solution was pumped at a flow rate of 7 mL/min. The light intensity obtained from the Xenon lamp (125 W, 420 nm) was determined to be 100 mW/cm^2. During illumination, 3 mL of the suspension was taken from the column at scheduled intervals. The Cr concentration prior to and after photocatalytic reduction was measured three times using a UV–vis/NIR spectrophotometer.

3. Results and discussions

3.1. Catalyst characteristics

The SEM and TEM images of photocatalytic material composed of PAN-CNT/TiO_2-NH_2 are shown in Fig. 1. TiO_2 NPs are distributed on the surface of nanofibers, which confirms that TiO_2 NPs attached to the surface of nanofibers due to the crosslinking procedure. The composite nanofibers appear smooth and uniform with an average diameter of 126 ± 4 nm.

In order to confirm the surface functionalization of the fabricated composite nanofibers, FTIR spectra of PAN nanofibers, and PAN-CNT/TiO_2-NH_2 composite nanofibers before and after

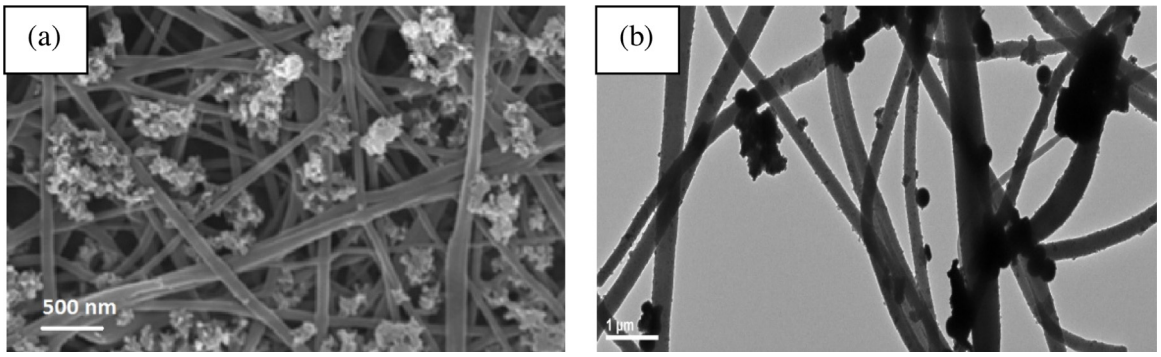

Fig. 1. (a) SEM and (b) TEM micrograph of PAN-CNT/TiO_2-NH_2 composite nanofibers.

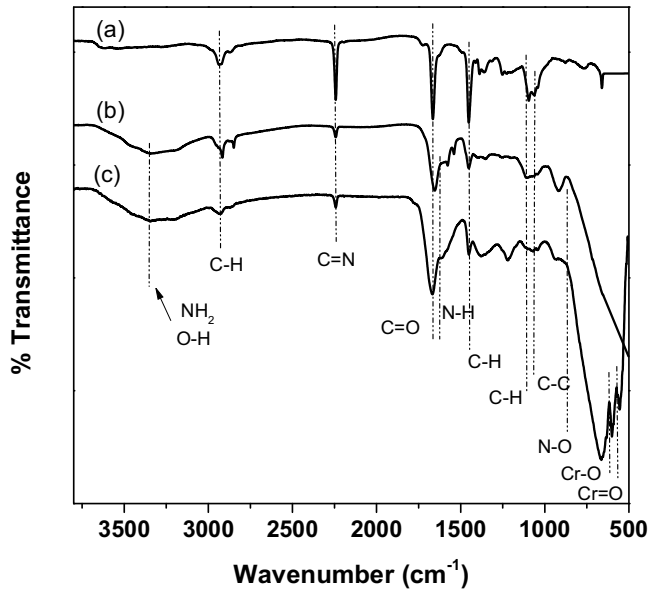

Fig. 2. FTIR spectra of (a) PAN (b) PAN-CNT/TiO_2-NH_2 and (c) PAN-CNT/TiO_2-NH_2 loaded with Cr(VI).

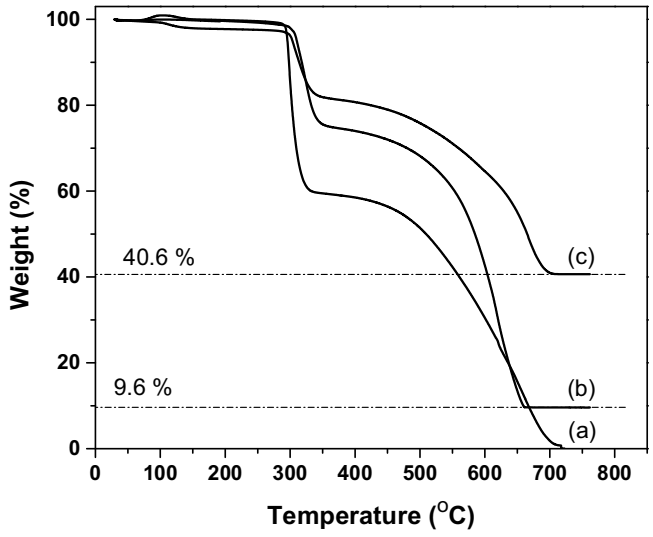

Fig. 3. TGA thermograms of (a) PAN nanofibers, (b) PAN-CNT nanofibers, and (c) PAN-CNT/TiO_2-NH_2 composites nanofibers.

the photoreduction of Cr(VI) were obtained as shown in Fig. 2. The spectrum for PAN nanofibers exhibited characteristic peaks of nitrile (2342 cm^{-1}), carbonyl (1700 cm^{-1}) and C—H stretching (3159 cm^{-1}) [40]. From Fig. 2b, the peak corresponding to nitrile is markedly decreased due to the conversion of nitrile to amidoxime, after the crosslinking of (PAN-CNT) to (TiO_2-NH_2). The absorption in the range 3100–3700 cm^{-1} is assigned to N—H and O—H vibrations. The bending vibrations of the amine group NH or NH_2 observed at 1680 cm^{-1} confirm the conversion of the nitrile group to amidoxime [41]. The band observed at 3159, 1520, and 1152 cm^{-1} assigned to the aliphatic C—H bending vibration of the CH_2 of polymeric chain, while the band observed at 900 cm^{-1} is assigned to N—O. After the photoreduction of Cr(VI) at pH 2, Fig. 2c two new peaks at 620 and 570 cm^{-1} appear in the FTIR spectrum of composite nanofibers, which are attributed to the Cr–O and Cr = O bonds from the Cr(VI) species. In addition, the band at 1200–1470 cm^{-1} corresponding to N—H and O—H bending is considerably increased due to the presence of Cr(VI) suggesting that the amine and oxime group of amidoxime are involved in the binding of chromium during Cr(VI) uptake [42].

Fig. 3 shows TGA thermograms of PAN nanofibers, PAN-CNT composites nanofibers, and PAN-CNT/TiO_2-NH_2 composites nanofibers in the temperature range from room temperature to 800 °C. The thermogram of PAN nanofibers shows three decomposition steps. In the first stage up to 290 °C, there was no weight loss. About, ~45% of weight loss was observed in the second stage from 290 °C to 300 °C, indicating that a significant chemical reaction took place, and volatile gasses evolved. In the last stage up to 720 °C, complete decomposition was observed. Furthermore, the weight of the PAN-CNT composite nanofibers decreased rapidly in the temperature range of 338–650 °C, due to the combustion and decomposition of composite nanofibers taking place at this temperature range. After the temperature was increased to 650 °C, the CNT remained and no more weight loss occurred, which meant that nanofibers were removed completely. For the PAN-CNT/TiO_2-NH_2 composite nanofibers, the weight decreased rapidly in the temperature range 338–705 °C, after that the TiO_2 remained and no more weight loss occurred, which meant that nanofibers were removed completely. Moreover, the TiO_2 content in the composites could be easily calculated from the weight remainder after the samples were heated over 705 °C. Since the sample PAN nearly completely disappeared over 720 °C, the CNT/TiO_2 and CNT contents in compositions were determined to be 40.6 wt% and 9.6 wt% for the sample PAN-CNT/TiO_2-NH_2 and PAN-CNT composite nanofibers, respectively.

3.2. *Photocatalytic performance of PAN-CNT/TiO_2-NH_2 composites nanofibers*

3.2.1. *Effect of catalyst content*

The amount of catalyst is an important parameter in optimizing the operational conditions. In this study, the effect of catalyst loading on the photoreduction of Cr(VI) was investigated using

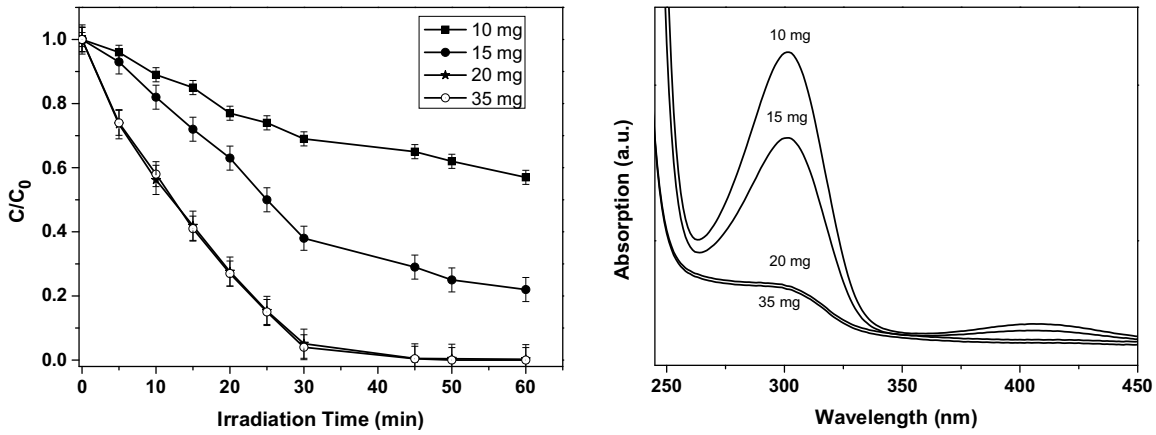

Fig. 4. Effect of catalyst dosage on photoreduction efficiency of Cr(VI) (Cr(VI) = 20 ppm, and pH 2).

a catalyst dosage (TiO_2/CNT) ranging from 10 to 35 mg to avoid an ineffective excess amount of the photocatalyst and the results obtained are shown in Fig. 4. The results indicate that the photoreduction efficiency of Cr(VI) gradually increases as the catalyst dosage increases from 10 to 35 mg. This may be attributed in terms of availability of the active sites on the photocatalyst surface and the penetration of visible light through the water, leading to an increase in the photoreduction of Cr(VI) [43,44].

3.2.2. Effect of irradiation time

In this study, the photoreduction activity of Cr(VI) using PAN-CNT/TiO_2-NH_2 and PAN/TiO_2-NH_2 composite nanofibers was investigated under the visible light as a function of the contact time. The photoreduction experiments of Cr(VI) were conducted at initial Cr(VI) concentration of 20 mg/L, pH 2 and the amount of photocatalyst is 20 mg. The results obtained are shown in Fig. 5. It can be seen that about 60% of photoreduction was achieved in less than 15 min irradiation time using PAN-CNT/TiO_2-NH_2 composites nanofibers, and a complete reduction was observed after 30 min. This may be due to the availability of more active binding sites on the surface of TiO_2 NPs that crosslinked to the composite nanofibers in order to increase the adsorption of Cr(VI), therefore enhance the photoreduction efficiency. Furthermore, the PAN-CNT/TiO_2-NH_2 composite nanofibers lead to high loading of Cr(VI) in a short time, due to increased active surface sites which will facilitate high exposure of light and then high photoreduction efficiency. According to previous studies under visible light at high power of 500 W [31–35], it takes about 2–4 h to get a complete photoreduction. On the other hand for the PAN/TiO_2-NH_2 composite nanofibers about 50% of photoreduction was achieved in less than 20 min irradiation time and no changes in the photoreduction efficiency were observed after 30 min irradiation time. These results indicated that the photocatalytic reduction efficiency increased with the incorporation of CNTs and TiO_2. This trend resulted from the high surface area of CNTs/TiO_2 photocatalytic. In addition, CNTs can effectively generate a greater number of electrons and holes, and accelerate the process of the photocatalytic reaction to enhance the photocatalytic activity. The photoreduction efficiency of Cr(VI) was determined from the results obtained from UV–vis spectroscopy. The results obtained are shown in Fig. 5b in which the peak at 350 nm corresponding to Cr(VI) was shifted to 302 nm, corresponding to Cr(III). The kinetic experiments data of the photocatalytic reduction of Cr(VI) are shown in Fig. 5c was successfully fitted well using commonly applied pseudo-first-order equation [45], which can be expressed as follows:

$$\ln\left(\frac{C_0}{C}\right) = k_a t \quad (1)$$

Where C_0 is the initial concentration of Cr (VI) and C is the concentration of Cr (VI) at a specific time, and k_a is the rate constant of pseudo-first order model (min^{-1}).

3.2.3. Effect of pH on the photoreduction of Cr(VI)

pH of the solution plays a major role in the photocatalytic process as it is known to influence the surface charge of the semiconductor thereby affecting the adsorption, interfacial electron transfer, and the photoreduction process [46]. The effect of pH on the photocatalytic reduction efficiency of Cr(VI) is presented in Fig. 6. As observed, the photoreduction efficiency of Cr(VI) was highly dependent on the pH with maximum photoreduction at pH = 2. The amount of Cr(VI) decreased in the aqueous solution with increasing pH. As seen from Fig. 6 that 100% photoreduction efficiency of Cr(VI) was obtained at pH 2. Then, the photoreduction of Cr(VI) decreased sharply to 72% as pH value increased to 9. The variation in reduction efficiency of Cr(VI) at different pH values may be attributed to the affinities of PAN-CNT/TiO_2-NH_2 composites nanofibers for the different species of Cr(VI) existing at acidic pH values namely $H_2CrO_4{}^0$, $HCrO_4{}^-$, $CrO_4{}^{2-}$, and $Cr_2O_7{}^{2-}$ [40]. The NH_2 groups on the surface of the TiO_2 nanoparticles can either be protonated to form $NH_3{}^+$ at low pH or be deprotonated to form $NH_2\cdots OH-$ at high pH. It is clear that negatively charged $HCrO_4{}^-$ and $Cr_2O_7{}^{2-}$ are easily to be adsorbed to the positively charged PAN-CNT/TiO_2-NH_2 composites nanofibers at low pH values due to the electrostatic attraction, therefore a higher yield of photoreduction [47,48]. The electrostatic repulsion between negative Cr(VI) species and negatively charged PAN-CNT/TiO_2-NH_2 composites nanofibers increased with increasing pH values, and thereby resulted in the decrease of the reduction of Cr(VI) [49]. To investigate the kinetics of Cr(VI) photoreduction under different pH values, the experimental data were successfully fitted using the pseudo-first order as shown in (Fig. S1, Supplementary data).

3.2.4. Effect of Cr(VI) initial concentration

The effect of initial Cr(VI) concentration on the photoreduction efficiency of Cr(VI) onto PAN-CNT/TiO_2-NH_2 composite nanofibers was studied at initial Cr(VI) concentration of 10–100 mg/L and pH = 2. The obtained result are shown in Fig. 7 shows that the photoreduction efficiency of Cr(VI) gradually decreases with the increase of the initial Cr(VI) concentration from 10 to 100 mg/L. The complete reduction can be achieved after 30 min at 10–20 mg/L initial Cr(VI) concentration, while the respective value decreases to 79% at 100 mg/L. A possible explanation has to do with the fact that increased Cr(VI) concentration increases the solution absorbance and, therefore, a greater fraction of the light is intercepted before reaching the catalyst surface, thus decreasing the degree of reduc-

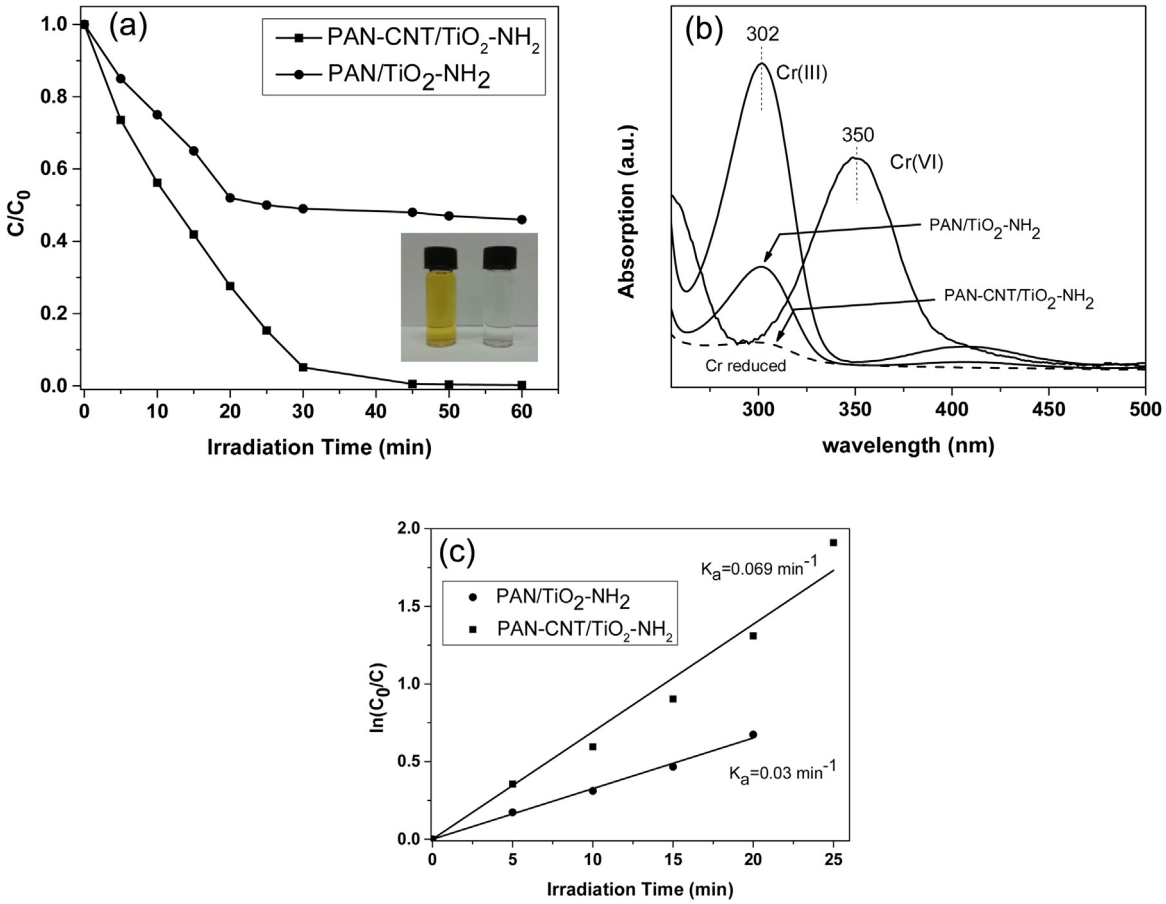

Fig. 5. (a) Photoreduction of Cr(VI) under visible light irradiation (b) UV–vis curves of Cr (VI) before and after photoreduction (c) Fitting of pseudo-first order model, (Cr (VI) = 20 ppm, pH = 2, catalyst amount = 20 mg).

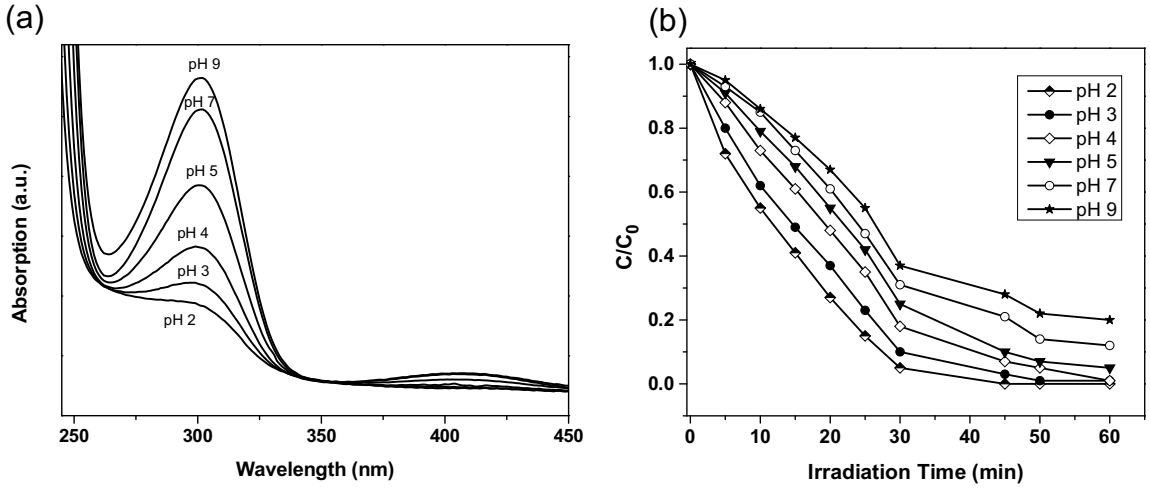

Fig. 6. (a) UV–vis spectra of photoreduction of Cr(VI) at different pH (b) Photoreduction of Cr(VI) at different pH onto PAN-CNT/TiO_2-NH_2 composite nanofibers.

tion [33]. The kinetic experiments for the photoreduction of various concentrations of Cr(VI) are shown in (Fig. S2, Supplementary data) was successfully fitted using pseudo-first-order. According to (Fig. S2, Supplementary data) with the increase of the initial concentration of Cr(VI), the rate constant k_a decreased. This can be attributed to the increase in Cr(VI) concentration, which decreases the path length of photons entering into the reaction mixture, and fewer photons reach the catalyst surface. In addition, the unchangeable value of light intensity, the amount of catalyst and irradiation time lead to the decrease of the availability of active sites. Consequently, the photoreduction efficiency of Cr(VI) decreases as the concentration increases [3,50,51]. Moreover, an increase in Cr(VI) concentration can lead to the saturation of the limited number of

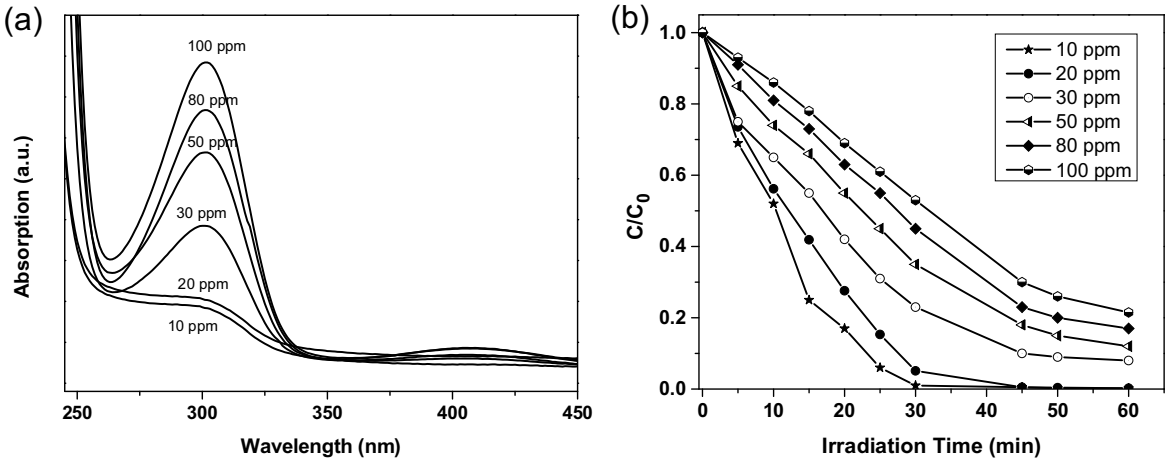

Fig. 7. (a) UV–vis spectra of photoreduction of Cr(VI) at different concentration (b) Photoreduction of Cr(VI) at different initial concentration onto PAN-CNT/TiO_2-NH_2 composite nanofibers.

accessible active sites on the photocatalyst surface, resulting in a reduction in the photoreduction efficiency.

3.2.5. XPS data analysis

In order to investigate the influence activity of the photocatalytic composite nanofibers on the photoreduction of Cr(VI), the composite nanofibers after adsorption step in the dark and the photoreduction step under visible light irradiation was directly examined by XPS. Fig. 8 shown the XPS patterns of the composite nanofibers, which showed the Cr 2p spectra recorded for Cr(VI) and Cr(III). As the Cr 2p peak is a doublet, the peak component at lower binding energy corresponds to Cr $2p_{3/2}$ orbital, while those at higher binding energy correspond to Cr $2p_{1/2}$ orbital. Before the photoreduction process took place, bands corresponding to Cr(VI) appeared at a binding energy of 579.2 and 588.3 eV, which confirms the adsorption of Cr(VI) on the surface of PAN-CNT/TiO_2-NH_2 composite nanofibers. After the irradiation of the nanocomposites with visible light, new significant bands appear corresponding to Cr(III) binding energy of 577.1 and 586.5 eV, which confirms the reduction of Cr(VI) to Cr(III) onto PAN-CNT/TiO_2-NH_2 composite nanofibers [52]. The wide-scan XPS spectrum shows also four peaks at 458.2 eV, 531.3 eV, 284.6 eV, and 399.3 eV corresponding to Ti 2p, O 1s, C 1s, and N 1s, respectively, indicating the existence of Ti, O, C, and N elements. The peaks in the Ti 2p spectrum at 458.2 eV and 464.1 eV represented to Ti $2p_{3/2}$ and Ti $2p_{1/2}$, respectively, indicating that titanium bounded to oxygen remains in oxidation state IV for the titanium-oxo cluster. The O1 s spectrum has a broad peak at 531.3 eV that is indicative of oxygen in metal oxides such as TiO_2. In addition, the peaks in the N 1 s region at 399.3 eV can be assigned to the N of the amine functionality.

3.2.6. Photoreduction of Cr(VI) in the presence of phenol

The PAN-CNT/TiO_2-NH_2 composite nanofibers was tested similarly to the industrial wastewater consists of a mixture of organic and inorganic pollutants. In this experiment, we tested the PAN-CNT/TiO_2-NH_2 composite nanofibers at 20 ppm of Cr(VI) aqueous solution and 20 ppm of phenol as a combination of pollutants in continuous mode [53,54]. Fig. 9 shows the kinetic first-order reaction for the degradation efficiency of phenol and the photoreduction of Cr(VI) in the absence or presence of phenol. This synergism is based on the photogenerated electrons and holes on the surface of the composite nanofibers [22–26]. The results indicated that the rate of Cr(VI) photoreduction was about 1.4 times higher in the presence of phenol than in its absence, which can be explained based on the mechanism as described in the following sections. Therefore, simultaneous redox reactions increase the efficiency of the reaction, with a concomitant decrease of water treatment cost.

3.2.7. Proposed reduction mechanism

The mechanism of photoreduction of Cr(VI) can be simplified schematically as shown in Fig. 10. The NH_2 groups on the surface of the TiO_2/CNT composite nanofibers can either be protonated to form NH_3 at low pH. It is clear that negatively charged Cr(VI) species are easy to be adsorbed to the positively charged TiO_2/CNT composite nanofibers at low pH values due to the electrostatic interaction. After visible light irradiation Cr(VI) reduced to Cr(III) on the surfaces of TiO_2/CNT composite nanofibers and release into the solution by electrostatic repulsion between the protonated surfaces of TiO_2/CNT and the cation Cr(III). The photoreduction of Cr(VI) achieved under visible light, where TiO_2/CNT NPs leads to the generation of electron-hole pairs at the surface of the photocatalyst (Eq 2). After the migration of electron-hole pairs to the surface of the particles, the photogenerated electrons reduce Cr(VI) to Cr(III) (Eq. (3)), and the holes may lead to generation of O_2 (Eq. (4)) and produce •OH radicals in the absence of any organics (Eq. (5)) [55]. Phenol can scavenge the valence band hole in the photocatalytic reaction system leading to an inhibition of recombination of electron and hole pairs on the catalyst surface and accelerating the reduction of Cr(VI) by photogenerated electrons [56]. In the presence of phenol, the holes can produce •OH radicals more than in the presence of Cr(VI), which can further degrade the phenol to CO_2 and H_2O (Eq. (6)) [57]. Therefore, the holes can also directly oxidize the phenol (Eq. (7)).

$$TiO_2/CNT + h\upsilon \rightarrow h^+ + e^- \quad (2)$$

$$Cr_2O_7^{2-} + 14H^+ + 6e^- \rightarrow 2Cr^{3+} + 7H_2O \quad (3)$$

$$2H_2O + 4h^+ \rightarrow O_2 + 4H^+ \quad (4)$$

$$H_2O + h^+ \rightarrow {}^\bullet OH + H^+ \quad (5)$$

$$^\bullet OH + \text{Phenol} \rightarrow CO_2 + H_2O \quad (6)$$

$$H^+ + \text{Phenol} \rightarrow CO_2 + H_2O \quad (7)$$

3.2.8. Catalyst reuse

The reuse of the catalyst is considered as an important aspect and an economic necessity. In these experiments, the PAN-CNT/TiO_2-NH_2 composite nanofibers were used in consecutive photocatalytic conditions in order to evaluate the durability of the composite nanofibers. At the end of each cycle, the composite

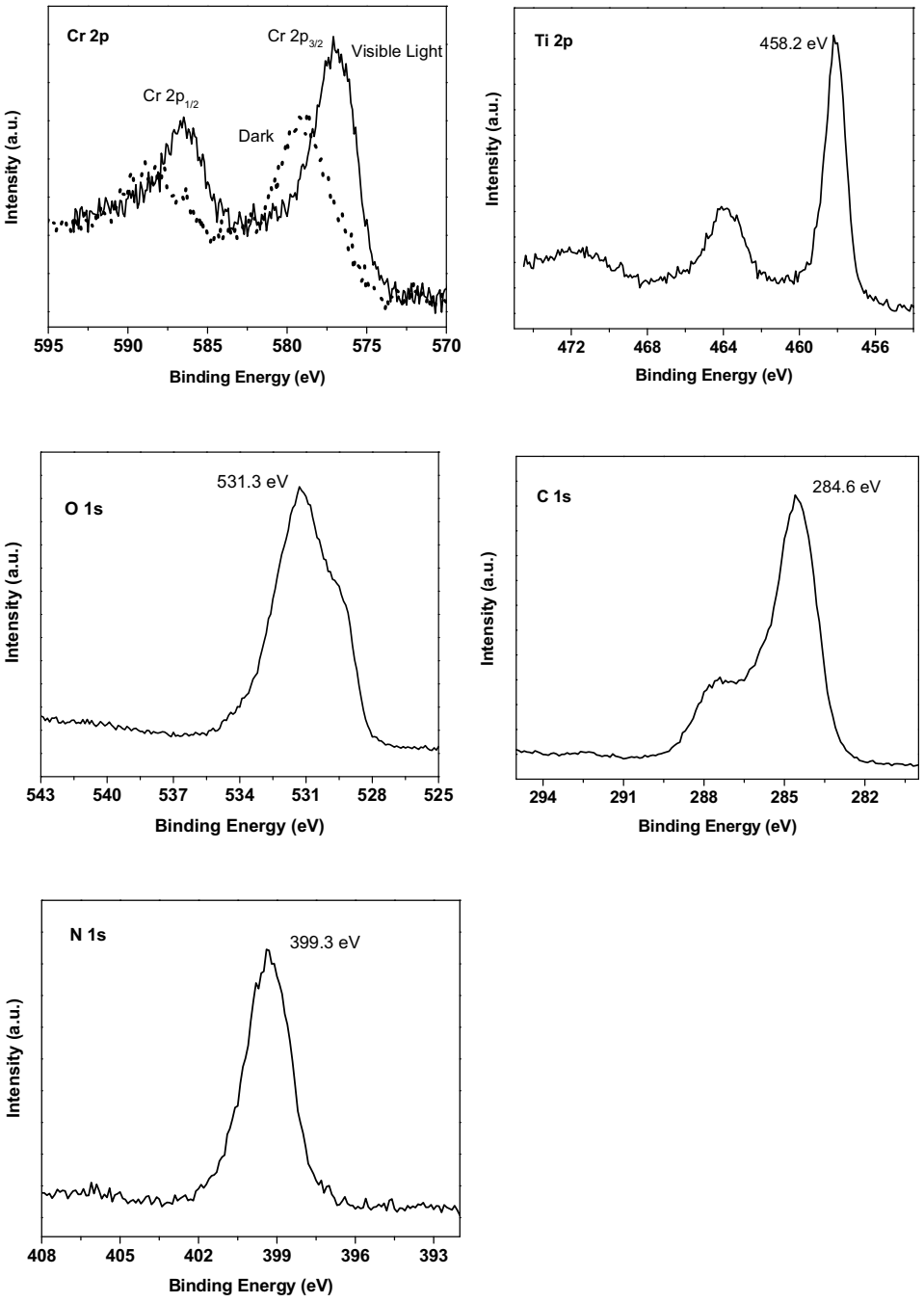

Fig. 8. XPS spectra of the PAN-CNT/TiO_2-NH_2 composite nanofibers for Cr(VI) before and after photocatalytic reduction process.

nanofibers was washed with deionized water and then dried in air. The photoreduction efficiency of PAN-CNT/TiO_2-NH_2 composites nanofibers slightly decreased with the cycle number repeated as shown in Fig. 11. After five consecutive adsorption-photoreduction cycles, the photoreduction efficiency of the composites nanofibers decreased by about 3%, which implies that the catalyst retained its photoreduction activity for Cr(VI). The slight decrease of the photoreduction performance of the PAN-CNT/TiO_2-NH_2 composites nanofibers might be due to the adsorption of the Cr(III) generated after photocatalytic reactions, which results in the decrease of adsorption and active sites on the surface of PAN-CNT/TiO_2-NH_2 composites nanofibers. These results have demonstrated that the good stability and reusability property would greatly promote the practical applications of composite nanofibers in the reduction of heavy metal pollutants from wastewater.

4. Conclusions

According to the results obtained in this work, the fabricated composite nanofibers display promising photocatalytic reduction efficiency for Cr(VI) in aqueous solution under visible light irradiation. The kinetics of the photoreduction process showed that complete photoreduction was achieved after approximately 30 min and the experimental data followed a pseudo-first-order model. The photoreduction efficiency of Cr(VI) was higher in acidic solutions than that in alkaline solutions due to the Cr(VI) species and

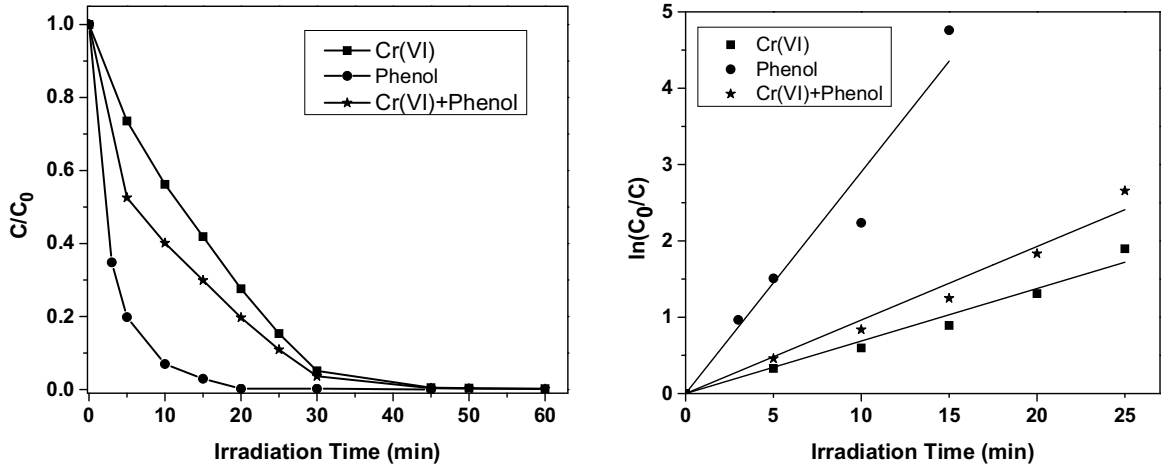

Fig. 9. Photoreduction of Cr(VI) in the absence or presence of phenol. (Cr(VI) = 20 ppm, phenol = 20 ppm, catalyst amount = 20 mg, and pH 2).

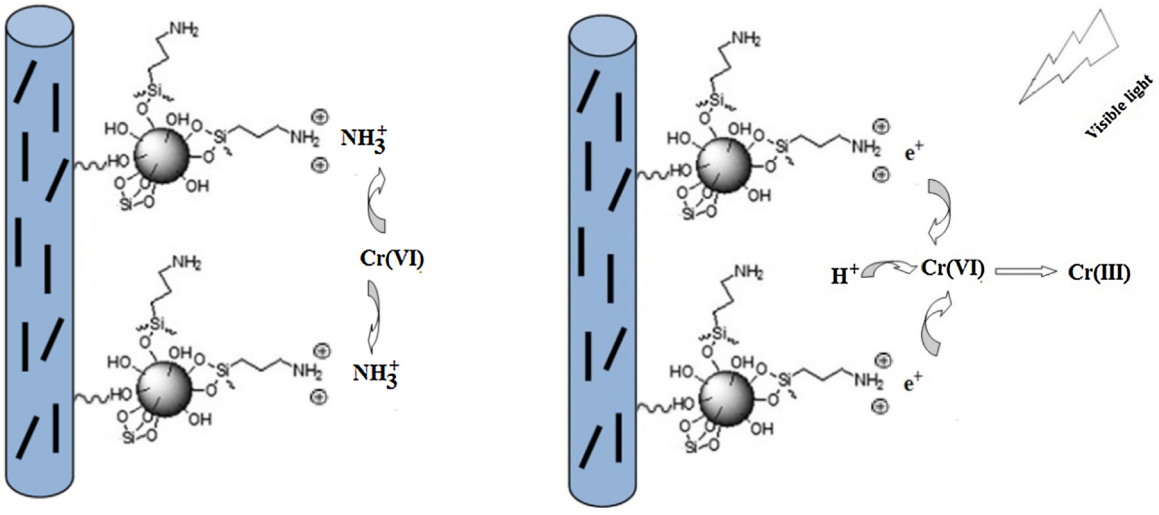

Fig. 10. Proposed mechanism of photocatalytic reduction of Cr(VI) under visible-light irradiation.

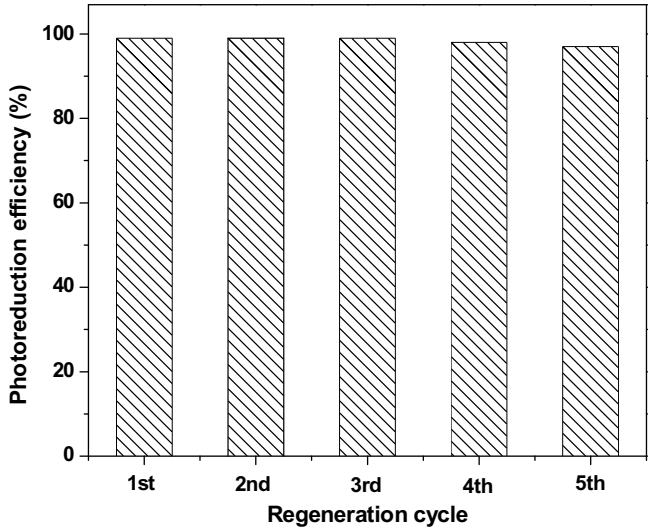

Fig. 11. Reusability of the composite nanofibers for the photoreduction of Cr(VI).

the protonation degree of the photocatalytic surface. The addition of phenol enhances the photoreduction of Cr(VI), due to its ability to adsorb on the catalyst surface, which can also act as a hole scavenger. The UV–vis spectrophotometer and XPS analyses proved that chromate Cr(VI) was reduced to Cr(III). Furthermore, the flexibility and the reuse of the PAN-CNT/TiO_2-NH_2 composite nanofibers, reveal their promising potential for advanced wastewater treatment.

Appendix A. Supplementary data

Supplementary data associated with this article can be found, in the online version, at http://dx.doi.org/10.1016/j.molcata.2016.08.010.

References

[1] L. Khezami, R. Capart, Removal of chromium(VI) from aqueous solution by activated carbons: kinetic and equilibrium studies, J. Hazard. Mater. 123 (1–3) (2005) 223–231.
[2] X. Guo, et al., High-Performance and reproducible polyaniline Nanowire/Tubes for removal of Cr(VI) in aqueous solution, J. Phys. Chem. C 115 (5) (2011) 1608–1613.
[3] Y. Ku, I.-L. Jung, Photocatalytic reduction of Cr(VI) in aqueous solutions by UV irradiation with the presence of titanium dioxide, Water Res. 35 (1) (2001) 135–142.
[4] M. Wang, M. Leitch, C. Xu, Synthesis of phenol–formaldehyde resol resins using organosolv pine lignins, Eur. Polym. J. 45 (12) (2009) 3380–3388.

[5] D. Fabbri, A.B. Prevot, E. Pramauro, Effect of surfactant microstructures on photocatalytic degradation of phenol and chlorophenols, Appl. Catal. B: Environ. 62 (1–2) (2006) 21–27.
[6] L.B. Khalil, W.E. Mourad, M.W. Rophael, Photocatalytic reduction of environmental pollutant Cr(VI) over some semiconductors under UV/visible light illumination, Appl. Catal. B: Environ. 17 (3) (1998) 267–273.
[7] F. Jiang, et al., Aqueous Cr(VI) photo-reduction catalyzed by TiO2 and sulfated TiO2, J. Hazard. Mater. 134 (1–3) (2006) 94–103.
[8] Y.C. Sharma, Effect of temperature on interfacial adsorption of Cr(VI) on wollastonite, J. Colloid Interface Sci. 233 (2) (2001) 265–270.
[9] R.J. Kieber, G.R. Helz, Indirect photoreduction of aqueous chromium(VI), Environ. Sci. Technol. 26 (2) (1992) 307–312.
[10] J. Doménech, J. Muñoz, Photocatalytical reduction of Cr(VI) over ZnO powder, Electrochim. Acta 32 (9) (1987) 1383–1386.
[11] Y. Zhang, J.C. Crittenden, D.W. Hand, The solar photocatalytic decontamination of water, Chem. Ind. 18 (1994) 714–717.
[12] Z. Yao, et al., Photocatalytic reduction of potassium chromate by Zn-doped TiO2/Ti film catalyst, Appl. Surf. Sci. 256 (6) (2010) 1793–1797.
[13] P. Mohapatra, S.K. Samantaray, K. Parida, Photocatalytic reduction of hexavalent chromium in aqueous solution over sulphate modified titania, J. Photochem. Photobiol. A: Chem. 170 (2) (2005) 189–194.
[14] J.A. Navío, et al., Heterogeneous photocatalytic reactions of nitrite oxidation and Cr(VI) reduction on iron-doped titania prepared by the wet impregnation method, Appl. Catal. B: Environ. 16 (2) (1998) 187–196.
[15] B. Sun, E.P. Reddy, P.G. Smirniotis, Visible light Cr(VI) reduction and organic chemical oxidation by TiO2 photocatalysis, Environ. Sci. Technol. 39 (16) (2005) 6251–6259.
[16] G. Bidoglio, et al., Humic acid binding of trivalent Tl and Cr studied by synchronous and time-resolved fluorescence, Environ. Sci. Technol. 31 (12) (1997) 3536–3543.
[17] D. Chen, F. Li, A.K. Ray, External and internal mass transfer effect on photocatalytic degradation, Catal. Today 66 (2–4) (2001) 475–485.
[18] D.S. Bhatkhande, V.G. Pangarkar, A.A.C.M. Beenackers, Photocatalytic degradation for environmental applications –a review, J. Chem. Technol. Biot. 77 (1) (2002) 102–116.
[19] J. Liqiang, et al., Review of photoluminescence performance of nano-sized semiconductor materials and its relationships with photocatalytic activity, Sol. Energy Mater. Sol. Cells 90 (12) (2006) 1773–1787.
[20] M.M. Rashad, et al., Synthesis and characterization of mesoporous anatase TiO2 nanostructures via organic acid precursor process for dye-sensitized solar cells applications, J. Ind. Eng. Chem. 19 (6) (2013) 2052–2059.
[21] M.a.T. De Volder, S.H. Baughman, R.H. Hart, AJ Carbon nanotubes: present and future commercial applications, Science 339 (2013) 535–539.
[22] R. Leary, A. Westwood, Carbonaceous nanomaterials for the enhancement of TiO2 photocatalysis, Carbon 49 (3) (2011) 741–772.
[23] Y. Liu, et al., Engineering highly active TiO2 photocatalysts via the surface-phase junction strategy employing a titanate nanotube precursor, J. Catal. 310 (2014) 16–23.
[24] A. Kongkanand, R. Martínez Domínguez, P.V. Kamat, Single wall carbon nanotube scaffolds for photoelectrochemical solar cells: capture and transport of photogenerated electrons, Nano Lett. 7 (3) (2007) 676–680.
[25] W. Feng, et al., Synthesis and characterization of nanofibrous hollow microspheres with tunable size and morphology via thermally induced phase separation technique, RSC Adv. 5 (76) (2015) 61580–61585.
[26] A.B. Sulong, M. Nurhamidi, Jaafar Sahari, Rizauddin Ramli, Baba Md. Dero, Joohyuk Park, Electrical conductivity behaviour of chemical functionalized MWCNTs epoxy nanocomposites, Eur. J. Sci. Res. 29 (1) (2009) 13–21.
[27] H. Guo, et al., Polyacrylonitrile/Carbon nanotube composite films, ACS Appl. Mater. Interfaces 2 (5) (2010) 1331–1342.
[28] H. Kuang-Ting, A. Justin, G.A. Suresh, Use of epoxy/multiwalled carbon nanotubes as adhesives to join graphite fibre reinforced polymer composites, Nanotechnology 14 (7) (2003) 791.
[29] A.K.-T. Lau, D. Hui, The revolutionary creation of new advanced materials—carbon nanotube composites, Compos. Part B: Eng. 33 (4) (2002) 263–277.
[30] D.J. Lipomi, Z. Bao, Stretchable, elastic materials and devices for solar energy conversion, Energy Environ. Sci. 4 (9) (2011) 3314–3328.
[31] C. Zhang, et al., Polyacrylonitrile/manganese acetate composite nanofibers and their catalysis performance on chromium (VI) reduction by oxalic acid, J. Hazard. Mater. 229–230 (2012) 439–445.
[32] Y.A. Shaban, Effective photocatalytic reduction of Cr(VI) by carbon modified (CM)-n-TiO2 nanoparticles under solar irradiation, World J. Nano Sci. Eng 3 (2013) 154–160.
[33] H. Wang, et al., Facile synthesis of amino-functionalized titanium metal-organic frameworks and their superior visible-light photocatalytic activity for Cr(VI) reduction, J. Hazard. Mater. 286 (2015) 187–194.
[34] Q. Wu, et al., Photocatalytic reduction of Cr(VI) with TiO2 film under visible light, Appl. Catal. B: Environ. 142–143 (2013) 142–148.
[35] X. Zhang, et al., One-dimensional hierarchical heterostructures of In2S3 nanosheets on electrospun TiO2 nanofibers with enhanced visible photocatalytic activity, J. Hazard. Mater. 260 (2013) 892–900.
[36] A. Mohamed, et al., Composite nanofibers for highly efficient photocatalytic degradation of organic dyes from contaminated water, Environ. Res. 145 (2016) 18–25.
[37] T.A.O. Alaa Mohamed, M.S. Toprak, M. Muhammed, A. Uheida, Efficient composite nanofibers for solar photocatalytic degradation of organic dyes and pharmaceutical drug, Appl. Catal. B: Environ. (2016).
[38] A. Mohamed, et al., Tribological behavior of carbon nanotubes as an additive on lithium grease, J. Tribol. 137 (1) (2014) 011801.
[39] C. Xiang, et al., Experimental and statistical analysis of surface charge: aggregation and adsorption behaviors of surface-functionalized titanium dioxide nanoparticles in aquatic system, J. Nanopart. Res. 15 (1) (2012) 1293–1304.
[40] M. Avila, et al., Surface functionalized nanofibers for the removal of chromium(VI) from aqueous solutions, Chem. Eng. J. 245 (2014) 201–209.
[41] L. Zhang, et al., Antimicrobial nano-fibrous membranes developed from electrospun polyacrylonitrile nanofibers, J. Membr. Sci. 369 (1–2) (2011) 499–505.
[42] S.H. Park, et al., Effects of iron catalyst on the formation of crystalline domain during carbonization of electrospun acrylic nanofiber, Synth. Met. 150 (3) (2005) 265–270.
[43] L. Wang, X. Jiang, Unusual catalytic effects of iron salts on phenol degradation by glow discharge plasma in aqueous solution, J. Hazard. Mater. 161 (2–3) (2009) 926–932.
[44] C.M. Ling, A.R. Mohamed, S. Bhatia, Performance of photocatalytic reactors using immobilized TiO2 film for the degradation of phenol and methylene blue dye present in water stream, Chemosphere 57 (7) (2004) 547–554.
[45] D.P. Das, K. Parida, B.R. De, Photocatalytic reduction of hexavalent chromium in aqueous solution over titania pillared zirconium phosphate and titanium phosphate under solar radiation, J. Mol. Catal. A: Chem. 245 (1–2) (2006) 217–224.
[46] M.-C. Lu, et al., Factors affecting the photocatalytic degradation of dichlorvos over titanium dioxide supported on glass, J. Photochem. Photobiol. A: Chem. 76 (1–2) (1993) 103–110.
[47] T. Karthikeyan, S. Rajgopal, L.R. Miranda, Chromium(VI) adsorption from aqueous solution by Hevea Brasilinesis sawdust activated carbon, J. Hazard. Mater. 124 (1–3) (2005) 192–199.
[48] N. Wang, et al., Synergistic effects of cupric and fluoride ions on photocatalytic degradation of phenol, J. Photochem. Photobiol. A: Chem. 191 (2–3) (2007) 193–200.
[49] R. Liang, et al., NH2-mediated indium metal–organic framework as a novel visible-light-driven photocatalyst for reduction of the aqueous Cr(VI), Appl. Catal. B: Environ. 162 (2015) 245–251.
[50] H. Chen, et al., Effective catalytic reduction of Cr(VI) over TiO2 nanotube supported Pd catalysts, Appl. Catal. B: Environ. 105 (3–4) (2011) 255–262.
[51] H. Mekatel, et al., Photocatalytic reduction of Cr(VI) on nanosized Fe2O3 supported on natural Algerian clay: characteristics, kinetic and thermodynamic study, Chem. Eng. J. 200–202 (2012) 611–618.
[52] M. Bhaumik, et al., Removal of hexavalent chromium from aqueous solution using polypyrrole-polyaniline nanofibers, Chem. Eng. J. 181–182 (2012) 323–333.
[53] J.J. Testa, M.A. Grela, M.I. Litter, Experimental evidence in favor of an initial one-Electron-Transfer process in the heterogeneous photocatalytic reduction of Chromium(VI) over TiO2, Langmuir 17 (12) (2001) 3515–3517.
[54] S.G. Schrank, H.J. José, R.F.P.M. Moreira, Simultaneous photocatalytic Cr(VI) reduction and dye oxidation in a TiO2 slurry reactor, J. Photochem. Photobiol. A: Chem. 147 (1) (2002) 71–76.
[55] L. Huang, et al., The simultaneous photocatalytic degradation of phenol and reduction of Cr(VI) by TiO2/CNTs, J. Ind. Eng. Chem. 18 (1) (2012) 574–580.
[56] A.D. Mani, et al., Facile synthesis of efficient visible active C-doped TiO2 nanomaterials with high surface area for the simultaneous removal of phenol and Cr(VI), Mater. Res. Bull. 61 (2015) 391–399.
[57] A. Al-Hamdi, M. Sillanpää, J. Dutta, Intermediate formation during photodegradation of phenol using lanthanum doped tin dioxide nanoparticles, Res. Chem. Intermed. 2015 (2016) 1–15.